

The Spontaneous Magnetic Field Generation and Suppression of Heat Conduction in Clusters of Galaxies

Nobuhiro Okabe and Makoto Hattori

Astronomical Institute, Tohoku University

We show that magnetic fields are spontaneously generated in the plasmas which have the temperature inhomogeneity and the heat conduction is spontaneously suppressed. This is based on the microscopic plasma instability that the anisotropic velocity distribution induced by the temperature gradient derives the low frequency growing transverse magnetic waves. We have shown that the physical mechanism for this growth is identical to the Weibel instability. The saturation level for this mode is determined by the wave-particle interaction. The results are applied to spatial variations of the plasma temperature in clusters and cold fronts which are bow-shaped contact surfaces between two different entropy plasmas, newly discovered structures by the Chandra X-ray observatory. We predict the existence of $10 \mu\text{G}$ magnetic fields along cold fronts. The predicted fields agree surprisingly well with those required to suppress the Kelvin-Helmholtz instability arising from the motion of fronts. Since magnetic fields are generated most strongly in the perpendicular direction to the temperature gradients, the heat conduction is significantly suppressed. Our field generation mechanism predicts the existences of $0.1\text{--}1 \mu\text{G}$ intracluster magnetic fields which are consistent with the observations of the synchrotron radio halos and the inverse Compton X-ray emissions.

1. Introduction

The presence of cluster magnetic fields is well established from different observational methods. Some clusters of galaxies have been reported to contain diffuse synchrotron radio emissions, called radio halos or relics. The volume-averaged magnetic field strengths in radio halos and relics can be estimated, assuming minimum energy arguments which roughly correspond to energy equipartition between relativistic particles and magnetic fields. Estimated strengths are about $0.1\text{--}1 \mu\text{G}$ (e.g., Govoni et al. 2001). These values are comparable to strengths evaluated by the combinations of the synchrotron radio emission with the hard X-ray emission which is interpreted as the inverse Compton scattering of the cosmic microwave background by the relativistic electrons (e.g., Rephaeli et al. 1999; Fusco-Femiano et al. 2003). Other observational studies are the Faraday rotation measurements of radio galaxies within or behind clusters. Faraday rotation derives magnetic field strengths along the line of sight, combined with the electron density n_e (e.g., Kim, Kronberg, & Tribble 1991; Clarke, Kronberg, & Böhringer 2001). The results yield that strengths of tangled magnetic fields are more than μG which is higher than those evaluated by both minimum energy arguments and inverse Compton X-ray observations. This discrepancy remains to be resolved.

In addition, new evidence of existence of magnetic fields along cold fronts is indirectly indicated by Vikhlinin et al. (2001b, 2002). Cold fronts are the bow-shaped discontinuities in the X-ray emitting hot plasmas in clusters of galaxies (Markevitch et al. 2000). The plasma temperature sharply increases across the disconti-

nities, while the plasma density sharply decreases across the discontinuities toward the same direction. They pointed out that a magnetic field of $10\mu\text{G}$ along the fronts should exist to explain the smoothness of the fronts otherwise the irregular structures are arisen by the Kelvin-Helmholtz (KH) instability.

Cluster magnetic fields are thought to be dynamically insignificant since magnetic energy is too small compared with the thermal energy. However, magnetic fields are expected to be playing important roles to reduce the classical Spitzer heat conductivity. The evidences of the suppression of heat conduction are shown in various environments of cluster plasma: in global temperature gradients (e.g., Fabian, Voigt, & Morris 2002; Zakamska & Narayan 2003), in temperature fluctuations which might be related to cluster mergers (e.g., Markevitch et al. 2003) and across cold fronts (e.g., Markevitch et al. 2000; Vikhlinin et al. 2001a). That indicates that the heat conductivity would be universally determined by the plasma physics. However, it is reported that the required reductions of heat conductivities are various. That would be due to the difference of plasma environments.

The origin of cluster magnetic fields has been discussed for a long time and many ideas were suggested (see Carilli & Taylor 2002, for a review). Early studies suggested that turbulences which are generated by galaxy motions in the intracluster medium (ICM) amplify the seed magnetic fields by dynamo actions. (e.g., Jaffe 1980; Ruzmaikin, A., Sokolov & Shukurov 1989). The seed fields are thought to be generated by Biermann's battery effect (Biermann 1950; Kulsrud et al. 1997). The field strengths are believed to be amplified up to the en-

ergy equipartition with the kinetic energy of turbulence, $B \leq \sqrt{4\pi\rho v^2}$, where ρ is the density and v is the velocity of the turbulence of plasma. However, dynamos by galaxy motions have the difficulty to explain cluster magnetic fields, since their predicted strengths are at most $0.1 \mu\text{G}$ (De Young 1992) and the regions where galaxies have moved seems to be uncorrelated with morphologies of the radio halos and relics. An alternative scenario with respect to dynamos is that cluster mergers drive turbulence and supply the magnetic energy with a small fraction of the merger energy. Another scenario that the magnetic fields are ejected from Active Galactic Nuclei is also difficult, because “bubble structures” as seen in Perseus (Fabian et al. 2000), A2052 (Blanton et al. 2001) and A2597 (McNamara et al. 2001) are not seen in clusters with radio halos or relics.

We proposed a new magnetic field generation mechanism. The proposed mechanism can realize the magnetic field along cold fronts (Okabe & Hattori 2003) required to suppress the KH instability (Vikhlinin et al. 2001b, 2002) and intracluster magnetic fields. Moreover, this mechanism has some powerful predictions, including the suppression of the heat conductivity.

The outline of the generation mechanism is as follows and the details are presented in each section: the electron velocity distribution function should deviate from a Maxwell-Boltzmann distribution function, since the heat flux always flows when the plasma has temperature gradients (in §2). Then, the low frequency transverse magnetic waves grow even in the absence of a background magnetic field (in §3). Since the instability was found by Ramani & Laval (1978), the instability is referred to as the Ramani-Laval (RL) instability in this paper. The applications of the RL instability to the cluster hot plasmas were examined by some authors; in cases of the plasma with background magnetic fields (Levinson & Eichler 1992) and the electron-ion two components plasma (Hattori & Umetsu 2000). We have shown that the mechanism of the RL instability is identical to the Weibel instability which is well-known as one of the mechanisms of magnetic fields generation (in §4). We found that the saturation level of RL instability is determined by the wave-particle interaction (Ramani & Laval 1978; Gallev & Natanzon 1991). The saturated magnetic fields will evolve into the large scales through an inverse cascade process, as reported in the numerical simulations of the Weibel instability (Lee 1973; Sentoku et al. 2000, 2002). These nonlinear evolutions of the RL instability are presented in §5.

We apply to clusters of galaxies and roughly estimate magnetic field strengths generated by the temperature gradients. We present these results in §6, predictions of our proposed mechanism and discussion in §7.

2. The Velocity Distribution Function in Plasma with Heat Flux

In this section, how the anisotropic electron velocity distribution function is set up when the temperature inhomogeneity exists in the plasma, is discussed from physical point of view. The absence of a background magnetic field is assumed. Consider the temperature inho-

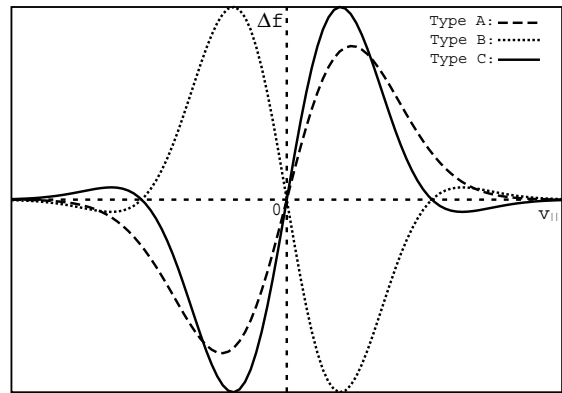


FIG. 1.— The possible candidates for the deviated part of the velocity distribution function from the Maxwell-Boltzmann.

mogeneity in hot electron plasma with the temperature variation scale of L . Since the heat conduction carries the heat flux from the hotter to cooler regions, the heat flux along the temperature gradient takes a negative finite value, $q \propto \langle v_{\parallel} v^2 f \rangle < 0$, where the bracket denotes the integral over the velocity space and the subscript \parallel denotes the component parallel to the temperature gradient. Therefore, the electron velocity distribution function, f , must deviate from the Maxwell-Boltzmann, $f_m = n_0(x_{\parallel})(\pi v_{\text{th}}(x_{\parallel})^2)^{-3/2} \exp(-v^2/v_{\text{th}}(x_{\parallel})^2)$; $\Delta f = f - f_m \neq 0$. Here, $n_0(x_{\parallel})$ is the electron number density, $v_{\text{th}}(x_{\parallel}) = (2k_B T(x_{\parallel})/m_e)^{1/2}$ is the thermal velocity with the temperature $T(x_{\parallel})$ and the electron mass m_e . The above condition together with $\langle \Delta f \rangle = 0$, the number density conservation, and $\langle v^2 \Delta f \rangle = 0$, the energy conservation, restricts the form of the deviated part, Δf , to be an odd function of the velocity component along the temperature gradient, v_{\parallel} . Of course, $\Delta f \rightarrow 0$ as $|v_{\parallel}| \rightarrow \infty$. In Figure 1, the possible cases of Δf are shown. From the zero current condition, $\langle v_{\parallel} \Delta f \rangle = 0$, the form like type A is rejected since Δf where $v_{\parallel} > 0$ and $v_{\parallel} < 0$ are respectively positive and negative, and $v_{\parallel} \Delta f > 0$ for all velocity and $\langle v_{\parallel} \Delta f \rangle > 0$. On the other hand, types B and C satisfy the zero current condition since the Δf curve crosses the v_{\parallel} -axis in each positive and negative v_{\parallel} region. The $\langle v_{\parallel} v^2 f \rangle$ for types B and C have finite values because this is the weighted mean of $\langle v_{\parallel} \Delta f \rangle$ weighted by v^2 , which is larger when $|v_{\parallel}|$ is larger. The heat flux condition of $\langle v_{\parallel} v^2 f \rangle < 0$ says that Δf should be positive where $v_{\parallel} \rightarrow -\infty$. Thus, type C is the only possible form as the deviated part in the plasma where a finite heat flow exists. The relative amplitude of the deviated part to the Maxwell-Boltzmann should be $\epsilon \delta T$, where $\epsilon = \lambda_{\text{mfp}}/L$ and $\delta T = \delta T/T$ is the fractional temperature fluctuation, since the deviation may be induced by Coulomb collisions and temperature fluctuations.

The deviated part Δf can also be deduced analytically. The Boltzmann equation is

$$\frac{\partial f}{\partial t} + v_{\parallel} \frac{\partial f}{\partial x_{\parallel}} - \frac{e}{m} E_{\parallel} \frac{\partial f}{\partial v_{\parallel}} = -\nu(f - f_m),$$

where E_{\parallel} is the zeroth electric field along the tempera-

ture gradient and the rhs is the Krook operator as the collision term and $\nu = (k_B T/m_e)^{1/2}/\lambda_e$ is the Coulomb collision frequency with the Coulomb mean free path λ_e (Sarazin 1988). Hereafter, we describe the collision frequency as $\nu = v_{\text{th}}/\lambda_{\text{mfp}}$ with the parameters $v_{\text{th}} = (2k_B T/m_e)^{1/2}$ and $\lambda_{\text{mfp}} = \sqrt{2}\lambda_e$. For simplicity, pressure balance is assumed. Then, $E_{\parallel} = 0$ (Ramani & Laval 1978). If the perturbative treatment is applicable to describe the system, the distribution function could be expanded in $\epsilon\delta_T$ as (Chapman & Cowling 1960),

$$f = f_m + \epsilon\delta_T f^{(1)} + \epsilon^2\delta_T^2 f^{(2)} \dots,$$

where $f^{(j)}$ ($j = 1, 2 \dots$) describe the deviation of the distribution function from the Maxwell-Boltzmann in order of $(\epsilon\delta_T)^j$. This expansion is known as the Chapman-Enskog expansion. Therefore, the electron distribution function up to the first order in $\epsilon\delta_T$ is obtained as

$$f = f_m \left[1 + \epsilon\delta_T \frac{v_{\parallel}}{v_{\text{th}}} \left(\frac{5}{2} - \frac{v^2}{v_{\text{th}}^2} \right) \right].$$

The form of the deviated part is essentially the same as type C shown in Figure 1. We note that adopting the Krook operator is not essential for determining the form of the deviated part.

3. Review of the RL Instability

The diagnostics of the Ramani-Laval (RL) instability are summarized, contrasting with the Weibel instability. As summarized in the Appendix, the temperature anisotropy excites the transverse magnetic waves due to the Weibel instability. The excited wave is a standing wave with zero phase velocity. The amplitude of the wave grows when the temperature perpendicular to the wave vector is higher than the temperature parallel to the wave vector. The amplitude of the wave is damped in the opposite situation.

Ramani & Laval (1978) studied the stability of the plasmas when the temperature distribution is not homogeneous. The non-equilibrium electron velocity distribution function is deduced from the assumed temperature distribution self-consistently using the Chapman-Enskog expansion. This is one of the prominent difference from the Weibel case, where the anisotropic electron velocity distribution function due to the temperature anisotropy is given by hand. The difference between the deduced non-equilibrium velocity distribution function and the equilibrium one, that is, the Maxwell-Boltzmann distribution, is that it is skewed in the direction of the temperature gradient and is the odd function of the velocity component along the temperature gradient. The velocity distribution functions in the both cases are anisotropic. However, the skewed nature found in the RL case is not found in the Weibel case. Although the anisotropic velocity dispersion is essential for the Weibel instability, the velocity dispersion is isotropic in the RL case. Ramani & Laval (1978) performed the linear stability analysis of the plasmas with the deduced non-equilibrium velocity distribution following the procedure of plasma kinetic theory. Two independent modes appear. The two modes are distinguished whether the magnetic field is or is not

in the plane made by the temperature gradient and the wave vector, where the first one is named mode 2 and the second one is named mode 1. The dispersion relation of the both modes have a real part as

$$\omega_r = \frac{\epsilon\delta_T}{4} k v_{\text{th}} \cos\theta.$$

The imaginary part of the mode 1 is obtained as

$$\gamma = \frac{\epsilon^2\delta_T^2}{8\sqrt{\pi}} k v_{\text{th}} (3\cos^2\theta - 2\sin^2\theta) - \frac{1}{\sqrt{\pi}} \left(\frac{c}{\omega_p} \right)^2 k^3 v_{\text{th}},$$

and the imaginary part of the mode 2 is obtained as

$$\gamma = \frac{3\epsilon^2\delta_T^2}{8\sqrt{\pi}} k v_{\text{th}} \cos^2\theta - \frac{1}{\sqrt{\pi}} \left(\frac{c}{\omega_p} \right)^2 k^3 v_{\text{th}},$$

where ω_p is the electron plasma frequency, c is the speed of light and θ is the angle between the direction of the temperature gradient and the wave vector. The existence of the real part in the dispersion relation of the RL instability is one of the differences from the Weibel case. Since the phase velocity along the temperature gradient, $\omega_r/k\cos\theta = \frac{\epsilon\delta_T}{4} v_{\text{th}}$, only takes a positive value, the wave propagates only one way from the low temperature region to the high temperature region. Therefore, the excited waves do not carry the heat from the hot to the cold region. Although mode 2 is a pure transverse wave, the longitudinal component of the electric fields, E_k , has a non-zero value for mode 1 as

$$E_k \sim \frac{\epsilon\delta_T}{4} \sin\theta \frac{v_{\text{th}}}{c} B_z.$$

This is another prominent difference from the Weibel case. The wave grows the most rapidly when the wave vector is parallel to the temperature gradient. The wave is damped when the direction of the wave propagation is perpendicular to the temperature gradient. The dependence on k of the growth rate is the same as that of Weibel.

In the sense that the anisotropic velocity distribution is the driving force of the instability, both instabilities are similar and therefore the RL instability was said to be Weibel-like. However, there are plenty of the qualitative differences among the both instabilities as explained above. Therefore, both instabilities were distinguished in Gallev & Natanzon (1991), and we try to identify the physical mechanism of the RL instability in the next section.

4. The Physical Mechanism of the RL Instability

The physical mechanism of the RL instability can be understood from the nature of the velocity distribution function when a finite heat flow exists, as illustrated in Figure 2. In the following discussion, strictness of the numerical factor is ignored. The peak position is shifted towards the positive v_{\parallel} direction, and the amount of the shift is $v_{\parallel} \sim \epsilon\delta_T v_{\text{th}}$. The phase velocity of any low frequency magnetic transverse wave must be close to the velocity at which the distribution function has a peak value, otherwise a finite net electric current is induced by the wave magnetic fields. This explains why

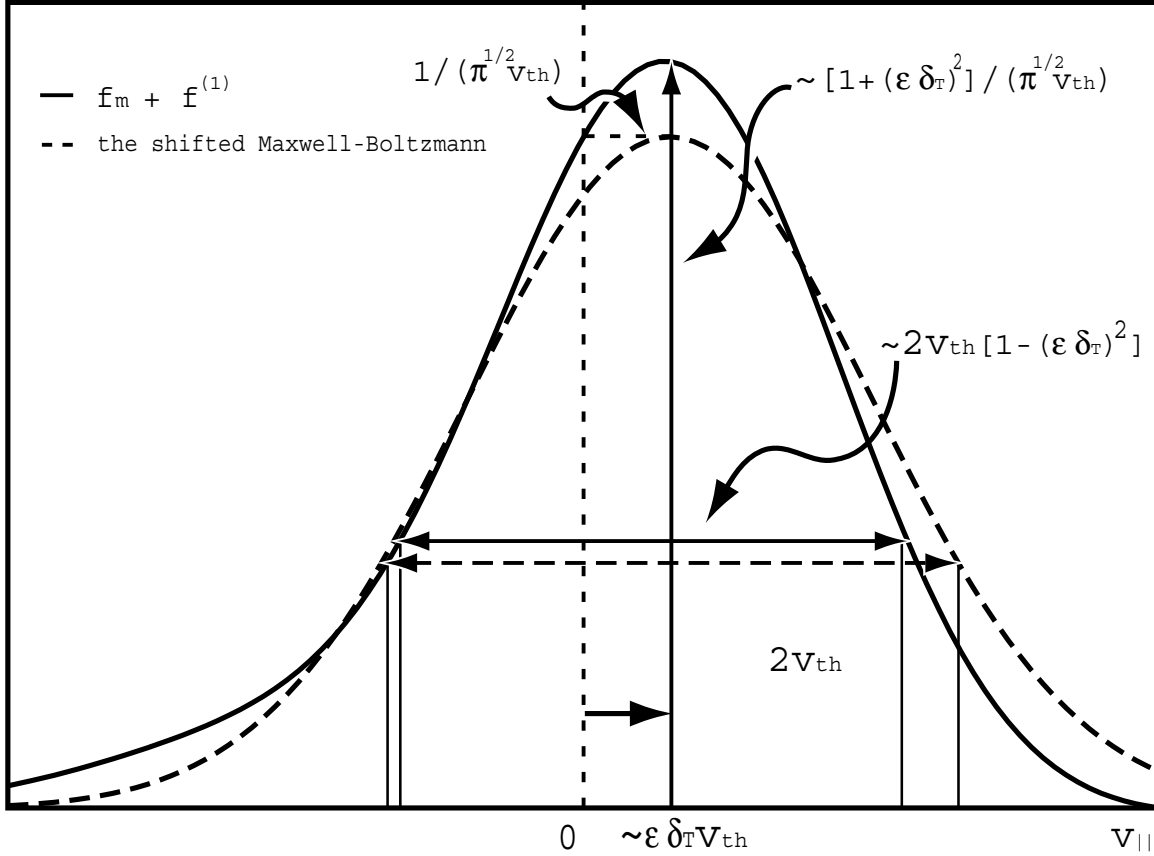


FIG. 2.— The solid line is the v_{\parallel} section of the total velocity distribution function $f_m + f^{(1)}$ in the plasma with the temperature gradient. The peak position is shifted by $\sim \epsilon \delta_T v_{th}$ from the Maxwell-Boltzmann. The peak value is increased by $\sim 1 + \epsilon^2 \delta_T^2$ compared with the Maxwell-Boltzmann. For comparison, the Maxwell-Boltzmann velocity distribution function shifted by $\sim \epsilon \delta_T v_{th}$ is shown as the dashed line. The velocity distribution function gets thinner in the v_{\parallel} direction. This can be interpreted as the decrease of the effective temperature by $\sim 1 - \epsilon^2 \delta_T^2$ in the direction of the temperature gradient.

the waves excited by the RL instability have a phase velocity of $\epsilon \delta_T v_{th}$, and travel only up the temperature gradient; the waves can not travel in the direction perpendicular to the temperature gradient. The waves excited by the Weibel instability are standing waves simply because there is no shift in the peak position of the velocity distribution function in the Weibel case. The peak value is increased by $\sim 1 + (\epsilon \delta_T)^2$ from that of the pure Maxwell-Boltzmann case since the amplitude of the deviated part takes a value of $\epsilon \delta_T v_{\parallel} \sim (\epsilon \delta_T)^2 v_{th}$ relative to the Maxwell-Boltzmann, and the value of the Maxwell-Boltzmann part is nearly same as the peak value at $v_{\parallel} \sim \epsilon \delta_T v_{th} \ll v_{th}$. Since the total electron number density must be unchanged, for the observer comoving with the waves this can be interpreted as a decrease in the effective electron temperature in the direction of the temperature gradient, T_{\parallel} , by $\sim 1 - (\epsilon \delta_T)^2$ relative to the temperature perpendicular to the temperature gradient, T_{\perp} (Fig. 2). The growth of the magnetic waves in the RL instability is therefore due to essentially the same mechanism as the Weibel instability (Weibel 1959; Fried 1959), in which the temperature anisotropy is the driving force of the instability. Consider the waves traveling nearly parallel to the temperature gradient. In this case,

$T_{\perp, \vec{k}} \sim T_{\perp}$ and $T_{\parallel, \vec{k}} \sim T_{\parallel}$, where $T_{\perp, \vec{k}}$ and $T_{\parallel, \vec{k}}$ are, respectively, the temperature components perpendicular to and parallel to the wave vector for an observer comoving with the waves. Since $T_{\perp, \vec{k}} > T_{\parallel, \vec{k}}$, the waves can grow. As a result, the direction of the magnetic field generated by the instability is almost perpendicular to the temperature gradient. The growth rate of the mode which travels toward the direction of the temperature gradient with wavenumber k is obtained from that of the Weibel instability (Krall 1973),

$$\begin{aligned} \gamma &\sim v_{th} \left[\left(\frac{T_{\perp}}{T_{\parallel}} - 1 \right) k - \left(\frac{ck}{\omega_p} \right)^2 k \right] \\ &\sim v_{th} \left[(\epsilon \delta_T)^2 k - \left(\frac{ck}{\omega_p} \right)^2 k \right]. \end{aligned}$$

The growth rate gets the maximum value of $\gamma_{max} \sim (\epsilon \delta_T)^3 (v_{th}/c) \omega_p$ at $k = k_{max} \sim \epsilon \delta_T \omega_p / c$. When the direction of the wave vector is perpendicular to the temperature gradient, $T_{\perp, \vec{k}} = T_{\parallel}$ and $T_{\parallel, \vec{k}} = T_{\perp}$. Since $T_{\perp, \vec{k}} < T_{\parallel, \vec{k}}$ in this case, the wave cannot grow. These results are exactly the same as the results of plasma kinetic theory, except for numerical factors (Ramani &

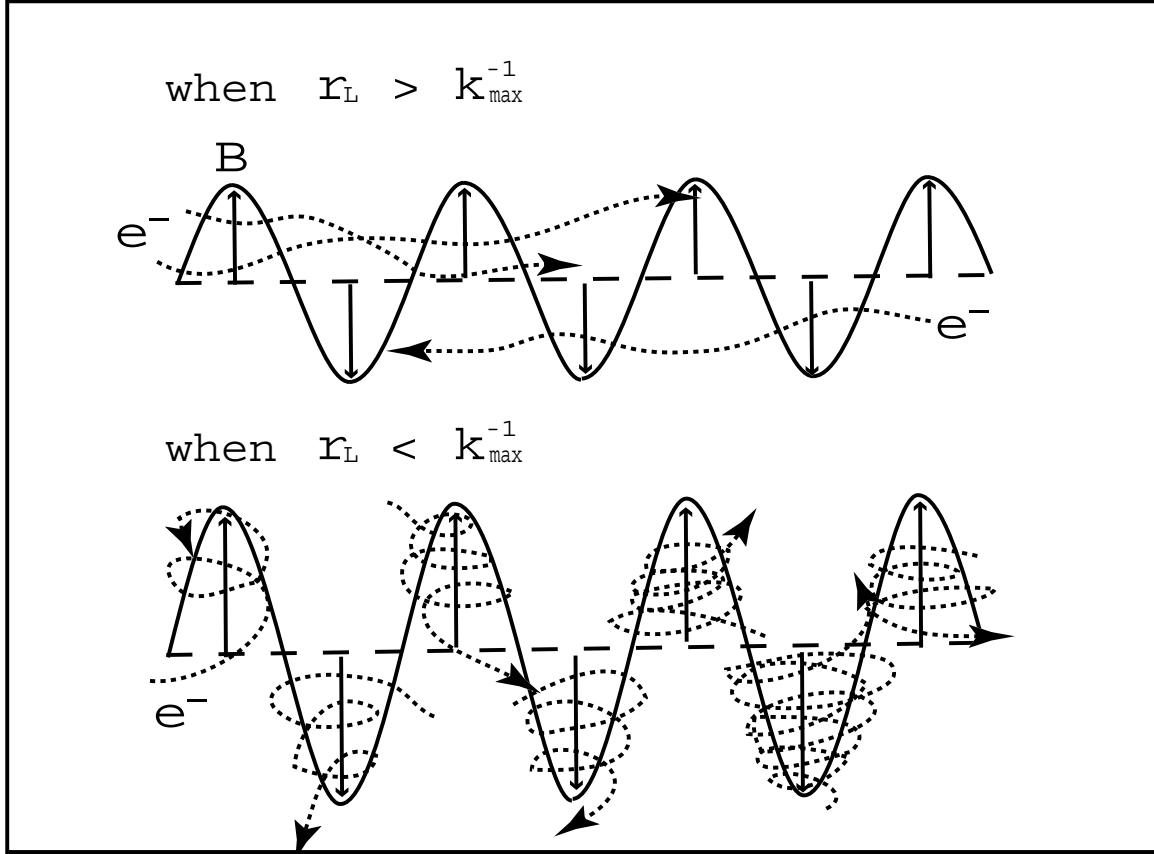


FIG. 3.— The nonlinear saturation by the wave-particle interaction. The top panel: When $r_L > k_{\max}^{-1}$, the thermal electrons travel throughout the waves but their orbits are randomly disturbed by the wavy magnetic fields. The bottom panel: Once r_L becomes smaller than k_{\max}^{-1} , the thermal electrons are trapped by the fields and feels net non zero fields.

Laval 1978; Hattori & Umetsu 2000; Okabe & Hattori in preparation).

The above discussion gives a complete physical explanation for mode 2 of the RL instability. However, these are not satisfactory for mode 1, in which the longitudinal electric field component appears. Unfortunately, we have not yet gotten the physical explanation for this. This is still an open question.

5. On the Nonlinear Evolution of the RL Instability

The nonlinear saturation level of the excited wave is estimated assuming that the wave-particle interaction determines the saturation level. The fundamentals are illustrated in Figure 3 (Ramani & Laval 1978; Gallev & Natanzon 1991). Once the Larmor radius of an electron gets shorter than the wavelength of the growing mode, the electron is trapped by the magnetic field of the wave, and the magnetic flux enclosed by its orbit becomes finite. Then, the kinetic energy of the trapped electron starts to monotonically increase as the growth of the magnetic field strength, since the increase of the magnetic flux enclosed by the electron orbit causes the induction of electric fields, which accelerate the electron as a betatron accelerator. Once the Larmor radius of typical thermal electrons, $r_L \sim v_{\text{th}} \omega_c^{-1}$, gets shorter than the wavelength of the fastest growing mode, that

is, $r_L k_{\max} < 1$, the increase of the kinetic energy of the electron system becomes significant if the waves still continue to grow. Since this violates the energy conservation, the growth of the magnetic field strength must be saturated when $r_L k_{\max} \sim 1$, that is, $B_s \sim \epsilon \delta_T \sqrt{\pi n_e k_B T}$.

The evolution of the magnetic fields after the nonlinear saturation could be described as follows. Some numerical simulations which follow the evolution of the Weibel instability showed that the strength of the magnetic field driven by the Weibel instability decreases after it gets the maximum value (Morse & Nielson 1971). This can be understood as follows. As the magnetic field grows, the electron velocity distribution become isotropic and it becomes difficult to maintain the electric current field which supports the magnetic field of the waves. In these simulations, the system is assumed to be isolated, and the initial anisotropic velocity distribution function is free to evolve to an isotropic one. On the other hand, in the case of the RL instability there is a driving force that maintains the anisotropy of the velocity distribution function. As long as the temperature gradient is not erased, the finite heat flux transports the heat from the hot to the cold region and the anisotropic velocity distribution function discussed in section 2 is maintained. Therefore, the decrease of the magnetic field strength after the nonlinear saturation as found in the Weibel instability may not occur in the RL instability. It is expected

that the generated magnetic field strength is kept at the saturated value for the lifetime of the temperature gradient. Wallace & Epperlein (1991) performed numerical simulations to follow the evolution of the Weibel instability when an initial anisotropic distribution function is maintained by an external source. They showed that the magnetic field strength is kept at a constant value after saturation. Their results support the above expectation for the RL instability. There are several indicative numerical simulations concerning the organization of the globally connected magnetic fields from the wavy fields generated by the instability. The wavy magnetic fields generated by the Weibel instability evolve into the longer wavelength modes after saturation (Lee 1973; Sentoku et al. 2000, 2002). This result indicates that the excited wavy magnetic fields automatically evolve into the globally connected fields. This could be understood as follows. After the magnetic field strength reaches the saturated level, the electric current field starts to behave as an individual electric beam every half wavelength (Fig. A4). Each beam is surrounded by the azimuthal magnetic field generated by the current beam itself. The electric beams interact each other via the Ampère’s force (Sentoku et al. 2000, 2002). The beams oriented in the same direction are attracted to each other and automatically gather. Finally, they merge into larger one beam. Since the physical mechanism of the growth of the RL instability is the same as the Weibel instability as shown in section 4, the same evolution is expected even in the RL case. The growth time scale of global magnetic fields is much longer than that of the linear phase.

Although the reduction of heat conductivity was originally considered due to the electrons scattering by the waves generated by the RL instability (Ramani & Laval 1978; Hattori & Umetsu 2000), this may not be the case. As discussed above, the wavy magnetic field generated by the instability could tend to form the global magnetic field automatically. Therefore, the suppression of heat conductivity may be determined by the trapping of the electrons by the organized magnetic field. To estimate the suppression of heat conductivity quantitatively, we need to know what is the final structure of the magnetic field due to self-organization. Detailed nonlinear studies, for example numerical simulations, are desired to answer the questions.

6. Applications to Clusters of Galaxies and Predictions

The *Chandra* X-ray observatory and *XMM-Newton* unveiled the various temperature structures in clusters of galaxies: global gradients, fluctuations, and sharp changes across cold fronts. Based on our proposed mechanism, self-organized magnetic fields can be generated in clusters with temperature gradients, since the time scale of inverse-cascading of the magnetic fields is expected to be short compared to the dynamical time scale. Therefore, we can estimate the generated magnetic field strengths from the observational data. Since the generated magnetic fields are ubiquitous in the temperature inhomogeneities, the saturated magnetic fields, $B_s \sim \epsilon \delta_T \sqrt{\pi n_e k_B T}$, can be compared with volume-

averaged strengths estimated by radio halos and relics or with inverse Compton hard X-ray emission. However, do not yet know the structure of generated fields, including the coherence length. Therefore, it is difficult to compare with results of Faraday rotation measurement, and we now focus on four clusters with cold fronts and diffuse radio emission—A3667, A2163, A754 and Coma. Although some of these clusters are not in pressure equilibrium, the estimated values of B_s under pressure equilibrium are not much different from those of the analysis that has no assumptions (Okabe & Hattori in preparation). Thus, we shall roughly estimate the saturated strength, B_s , from the X-ray data. We note that although we should use number densities and temperatures of plasma with no magnetic fields, using the data of clusters which have magnetic fields does not significantly change the estimate since the generated magnetic energy is much smaller than the thermal energy.

We adopt $H_0 = 50 \text{ km s}^{-1} \text{ Mpc}^{-1}$ and $q_0 = 0.5$ as cosmological parameters.

6.1. Cold Front in A3667

A3667 is a cold front cluster. The temperature and number density of the electrons change from $k_B T_c = 4.1 \pm 0.2 \text{ keV}$ and $n_{e,c} = 3.2 \pm 0.5 \times 10^{-3} \text{ cm}^{-3}$ to $k_B T_h = 7.7 \pm 0.8 \text{ keV}$ and $n_{e,h} = 0.82 \pm 0.12 \times 10^{-3} \text{ cm}^{-3}$ across the cold front (Vikhlinin et al. 2001a). The width of the cold front is $L \sim 5 \text{ kpc}$ at maximum. The Coulomb mean free path of the thermal electrons in the cold front region is $\lambda_e = 5.4(T/T_{\text{ave}})^2(n_e/n_{\text{ave}})^{-1} \text{ kpc}$, where $T_{\text{ave}} = (T_h + T_c)/2$ and $n_{\text{ave}} = (n_{e,h} + n_{e,c})/2$. Thus, $\epsilon \delta_T \sim 1$ in the cold front of A3667. The growth time scale of the unstable mode in the cold front is $\gamma_{\text{max}}^{-1} \sim 0.1 \text{ sec}$. Although it is difficult to estimate the exact time scale over which the instability can generate magnetic fields with the saturation value over the scale of the interface, it must be several tens of times longer than the growth time scale. Therefore, it is expected that the magnetic field is generated almost instantaneously compared with any other dynamical time scales in the cluster of galaxies. By applying the saturation level discussed in the previous section, the saturated magnetic field strength in the cold front should be $B_{s,\perp} \sim 8 (T/T_{\text{ave}})^{3/2}(n/n_{\text{ave}})^{-1/2} \mu\text{G}$. The obtained value agrees surprisingly well with the speculated value of $10 \mu\text{G}$ based on the stability consideration against the KH instability. The main direction of the generated magnetic field should be almost parallel to the cold front surface due to the characteristics of the mode. As discussed in section 5, the generated wavy magnetic fields could tend to evolve into the globally connected field. Therefore, we expect that the cold front surface is covered by the globally connected magnetic fields directed tangential to the surface with a strength of $10 \mu\text{G}$, and the KH instability is suppressed by these fields. The field strength required to suppress the KH instability is calculated using the tangential velocity at a angle $30^\circ \pm 10^\circ$ from the direction of the cold front motion Vikhlinin et al. (2001b). Therefore, it does not directly indicate the existence of magnetic fields at the center, much less all over the cold front. However, our model can explain the existence of such a strong field all

over the cold front where the temperature jump exists. The generated magnetic field could significantly reduce the electron mean free path in the direction of the temperature gradient and suppress heat conduction all over the cold front.

6.2. A2163

Abell 2163 is a distant rich cluster ($z = 0.203$). This cluster has a powerful radio halo. According to the VLA observation of Feretti et al. (2001), it has a regular shape and slight elongation in the E-W direction. Its total extent, which is the region filled by the relativistic particles, is $\sim 11.5' \sim 2.9$ Mpc. They also estimated the magnetic field strength by the minimum energy argument, $B_r \sim 0.9 \mu\text{G}$. On the other hand, a *Chandra* X-ray observation (Markevitch & Vikhlinin 2001) shows that the temperature is complicated. The temperature varies from two hot regions ($k_B T > 17$ keV and $k_B T > 16$ keV) to a cool core ($k_B T = 8.8$ keV). This complex temperature map is thought to be a result of cluster merging. The radial temperature profile shows that the temperature roughly varies by 1 keV over $1' \sim 256$ kpc in the region $r < 5'$. The electron number density profile was fitted with a β model

$$n_e(r) = n_0(1 + (r/r_c)^2)^{-3\beta/2},$$

where n_0 is the central electron number density, r is the radius, r_c is a characteristic scale (Elbaz, Arnaud & Böhringer 1995). Their result gives $n_0 = 6.65 \times 10^{-3} h_{50}^{1/2} \text{cm}^{-3}$, $\beta = 0.62$, $r_c = 1.20'$. So, the rough estimate of generated field strengths,

$$B_s \sim 1 \left(\frac{k_B \delta T / L}{0.004 \text{ keV kpc}^{-1}} \right) \left(\frac{T}{T_{\text{ave}}} \right)^{3/2} \times \left(\frac{n_e}{2 \times 10^{-3} \text{ cm}^{-3}} \right)^{-1/2} \mu\text{G}.$$

is in good agreement with B_r . Here, we use the average temperature $k_B T_{\text{ave}} = 12.3_{-1.1}^{+1.3}$ keV derived by Markevitch & Vikhlinin (2001) and the electron number density at $r \sim 2'$.

6.3. A754

Abell 754 is a rich cluster at $z = 0.0541$. The detailed temperature map is derived by a *Chandra* observation (Markevitch et al. 2003). It exhibits a complex temperature structure, which indicates that A754 is a merging cluster and that the X-ray emitting plasma is not in equilibrium. The temperature seems to vary at least by $k_B \delta T \sim 2$ keV within $l_T \sim 130$ kpc from their map. The average temperature $k_B T_{\text{ave}} = 10.0 \pm 0.3$ keV is obtained in $r < 9'$. The electron number density n_e fitted by the β model is obtained by Mason & Myers (2000): $n_0 = 2.69 \times 10^{-3} h_{50}^{1/2} \text{cm}^{-3}$, $\beta = 0.713$, $r_c = 5.50'$. So, the generated field strengths are roughly estimated as

$$B_s \sim 0.5 \left(\frac{k_B \delta T / L}{0.015 \text{ keV kpc}^{-1}} \right) \left(\frac{T}{T_{\text{ave}}} \right)^{3/2} \times \left(\frac{n_e}{10^{-3} \text{ cm}^{-3}} \right)^{-1/2} \mu\text{G},$$

where the electron density is adopted at $r \sim 6'$. On the other hand, the diffuse radio emission in A754 was examined Bacchi et al. (2003). It consists of a radio halo and a relic which are classified by whether there is cD galaxy in the radio emitting region or not. The region observed by *Chandra* coincides with the relic region. The magnetic field determined using a minimum energy argument is $B_r \sim 0.3 \mu\text{G}$. A hard X-ray excess is also detected by *Beppo SAX* at the 3.2σ level (Fusco-Femiano et al. 2003). Assuming that the origin is inverse Compton emission, they estimated that the magnetic fields is $B_i \sim 0.1 \mu\text{G}$. These observational values are consistent with the rough estimate of generated fields.

6.4. Coma

The temperature structure in the Coma cluster was derived by *XMM-Newton* observations (Arnaud et al. 2001; Briel et al. 2001). The radial temperature profile centered on NGC 4874 shows that the temperature around NGC 4874 sharply increases from about 6.5 keV to about 8.5 keV within $\sim 1.5' \sim 58$ kpc as the distance from NGC 4874 increases (Arnaud et al. 2001). On the whole, the temperature distribution is homogeneous, although locally it fluctuates slightly as seen in their temperature maps (Figure 5 in Arnaud et al. 2001 and Figure 3 in Briel et al. 2001). The electron density is given by a β model with $n_0 = 2.89 \times 10^{-3} h_{50}^{1/2} \text{cm}^{-3}$, $r_c = 10.5'$ and $\beta = 0.75$ Briel et al. (1992). So, around NGC 4874, the field strength generated by the RL instability is

$$B_s \sim 0.4 \left(\frac{k_B \delta T / L}{0.034 \text{ keV kpc}^{-1}} \right) \left(\frac{k_B T}{7.5 \text{ keV}} \right)^{3/2} \times \left(\frac{n_e}{2.9 \times 10^{-3} \text{ cm}^{-3}} \right)^{-1/2} \mu\text{G}.$$

Furthermore, we estimate that the fluctuations in temperature are 0.5 keV within $1'$, from Figure 7 in Arnaud et al. (2001). As a result, the field strength is estimated to be

$$B_s \sim 0.2 \left(\frac{k_B \delta T / L}{0.013 \text{ keV kpc}^{-1}} \right) \left(\frac{T}{T_{\text{ave}}} \right)^{3/2} \times \left(\frac{n_e}{2 \times 10^{-3} \text{ cm}^{-3}} \right)^{-1/2} \mu\text{G},$$

where $k_B T_{\text{ave}} = 8.25 \pm 0.10$ keV is the average temperature. The general techniques to estimate magnetic field strengths give us some results. Based on the minimum energy argument, a magnetic field of $B_r \sim 0.4 \mu\text{G}$ is determined from the giant radio halo (Giovannini et al. 1993). Rossi X-ray Timing Explorer (RXTE) measurements of hard X-ray emission, interpreted as inverse Compton scattering by relativistic electrons off the cosmic microwave background, lead to $B_i \sim 0.1\text{--}0.3 \mu\text{G}$ (Rephaeli, Gruber & Blanco 1999; Rephaeli & Gruber 2002). These observational results for B_r and B_i are the same order as the predicted strengths B_s .

7. Predictions and Discussion

We have successfully determined the physical mechanism responsible for one of the two independent modes

of the RL instability, and shown that the growth mechanism is identical to the Weibel instability which is well known as one of the generation mechanism of the magnetic field. Therefore, the RL instability can be also considered as the generation mechanism of the magnetic fields in astronomical situations. The nonlinear saturation level of the instability is estimated by considering the wave-particle interaction. The evolution of the magnetic fields after saturation are speculated on by referring to the previous numerical simulations which followed the non-linear evolution of the Weibel instability. The generated fields might be self-organized and evolve into the globally connected magnetic field.

We have applied the proposed mechanism to four clusters (A3667, A2163, A754, and Coma) and roughly estimated the typical strengths of magnetic fields generated by the RL instability, using projected temperature distributions. Although estimated strengths are rough and not volume averaged, the strengths of magnetic fields required agree with the observational results, except for the measurements of Faraday rotation. In the cold front cluster A3667, 10 μG magnetic fields along cold fronts are ubiquitous in the front. Here it is an important point that magnetic fields required from the viewpoint of hydrodynamics can be naturally explained by plasma kinetic theory. Regarding clusters with diffuse radio emission, predicted strengths agree well with 0.1–1 μG derived by minimum energy arguments and the combination of synchrotron and inverse Compton luminosity. Since temperature inhomogeneities exist in the radio emitting region, magnetic fields of the same order as the estimated values can exist all over radio halos and relics. Moreover, morphologies of radio halos and relics are expected to be associated with the temperature structure, since the regions where magnetic fields are generated are determined by temperature inhomogeneities. This prediction also corresponds to the apparent correlation between the radio brightness and the plasma temperature in A2163, pointed out by Markevitch & Vikhlinin (2001). On the other hand, the proposed mechanism cannot, at present, be compared with the measurement of Faraday rotation, since the final structure of generated fields, including the coherent length, is not clear. Therefore, further studies with respect to nonlinear evolution of the RL instability are necessary to unveil the topology of generated magnetic fields. For example, the application of the RL instability to Faraday rotation would provide us with the coherent lengths of generated fields. Another approach would be numerical simulations. If we know

the field structure, we can quantitatively calculate the self-regulated heat conductivity.

The predictions of the magnetic fields generation mechanism by the temperature gradients are summarized.

Predictions

- Our proposed mechanism can predict that 10 μG magnetic fields along cold fronts in A3667 exist all over the fronts, while the existence of fields required to suppress the KH instability is not indicated all over fronts.
- Magnetic fields required from the viewpoint of hydrodynamics can be naturally explained by plasma kinetic theory.
- Our proposed mechanism predicts the 0.1–1 μG magnetic fields derived by studies of radio halos and inverse Compton hard X-ray emission.
- Magnetic fields are ubiquitous in any astrophysical plasma with temperature inhomogeneities.
- The magnetic energy is determined by the plasma environment and is at equilibrium with the thermal energy via the RL instability.
- The morphologies of radio halos and relics are associated with that of the X-ray temperature map, since the regions where magnetic fields exist are determined by temperature inhomogeneities.
- The steep correlation between radio power P_ν and temperature $k_B T$ Liang et al. (2000) can also be explained (Okabe & Hattori in preparation).
- Magnetic field strengths don't depend on redshift because the evolution time scale of magnetic fields is short.
- The heat conduction could be self-regulated, since magnetic fields are generated by the plasma itself.

N. Okabe acknowledges travel support by the Hayakawa Satio Foundation in the Astronomical Society of Japan. The authors gratefully thank T. N. Kato, Y. Fujita, M. Takizawa, M. Iijima, and H. Ohno for a lot of fruitful comments.

Appendix

THE WEIBEL INSTABILITY

The Weibel instability is driven by an anisotropic temperature distribution and generates growing transverse magnetic standing waves (Weibel 1959). This instability is well known as the mechanism of magnetic field generation from zero initial magnetic field. Consider a plasma with an anisotropic temperature such as

$$f = n_0 \frac{1}{\pi^{3/2} v_{\text{th},\perp}^2 v_{\text{th},\parallel}} \exp \left[-\frac{v_{\parallel}^2}{v_{\text{th},\parallel}^2} - \frac{v_{\perp}^2}{v_{\text{th},\perp}^2} \right],$$

where the subscripts \parallel and \perp denote, respectively, the directions parallel and perpendicular to the wave vector. The dispersion relation is obtained by linear plasma kinetic theory (Krall 1973) as

$$\omega_r = 0,$$

$$\gamma = \frac{1}{\sqrt{\pi}} k v_{\text{th},\parallel} \frac{T_{\parallel}}{T_{\perp}} \left[\left(\frac{T_{\perp}}{T_{\parallel}} - 1 \right) - \left(\frac{kc}{\omega_p} \right)^2 \right].$$

The waves have no real part of the frequency. The waves grow when $T_{\perp} > T_{\parallel}$. The excited waves are transverse magnetic waves with no electric field.

The physical mechanism of the Weibel instability was first identified by Fried (1959). Consider the simple situations shown in Fig. A4. The electrons and their initial velocities are expressed as the filled circles and the dotted arrows. In case A, the simple anisotropic initial electron distribution function

$$f_0(\vec{v}) = n_0 w \delta(v_{\parallel}^2 - w^2) \delta(v_{\perp}) \delta(v_z)$$

is assumed. This represents the extreme case of $T_{\perp} = 0$, $T_{\parallel} \neq 0$. The directions of the perturbed magnetic fields are perpendicular to the paper: \odot and \otimes represent that the fields projected from the paper and into the paper, respectively. The size of the circle is proportional to the field strength at each position.

First, the qualitative explanation of the physical mechanism is reviewed. The electrons' orbits are deflected due to the introduction of the perturbed magnetic field as shown by the dashed arrows. The amount of the deflection is proportional to the field strengths at the each position. We first discuss the Case A. Consider the electrons (a) and (a') which initially have negative velocity in the x_{\perp} direction. They carry the positive electric currents in the x_{\perp} direction out of and into the shaded region, respectively. Because of the differences in the field strengths, the net positive current in the x_{\perp} direction is carried out from the region in a certain infinitesimal time interval. In other words a net negative electric current is carried into the region by the perturbed motion of these electrons. The electrons (b) and (b') also carry the a negative electric current into the shaded region. Therefore, a net negative electric current develops in the shaded region due to the injection of the perturbed magnetic field. Since the values of the induced electric currents are larger where the gradient of the magnetic field strength is larger, the current fields illustrated in Fig. A4 are set up, where the lengths of the arrows are proportional to the amplitudes of the currents. The magnetic field is produced around each electric current according to the Ampère's law as illustrated in Fig. A4. The growth of the magnetic field is determined by the superposition of these fields. For example, at point x_1 the net magnetic field generated by the current fields is normal to the paper toward the reader and amplifies the injected perturbed field. Since the excited fields amplify the injected perturbed fields everywhere, the perturbed field grows in Case A. On the other hand, the net induced electric currents in Case B are in the direction opposite those in Case A. Therefore, the perturbed magnetic field is damped in Case B. Hence, when $u > w$ ($T_{\perp} > T_{\parallel}$) the magnetic field perturbation grows, and when $u < w$ ($T_{\perp} < T_{\parallel}$) the magnetic field perturbation is damped. While this simple explanation shows qualitatively how the growth occurs, the role of electromagnetic induction for the growth of the instability, which was neglected in the above discussion, should be examined since it acts to reduce the growth of the magnetic field.

Next, a semi-quantitative explanation of the instability is given to see the role of induction. For this purpose, only case A is considered. Suppose that an initial perturbed magnetic field is

$$B_z = B e^{ikx_{\parallel}}.$$

The x_{\parallel} and x_{\perp} components of the equation of motion of the electron are given by

$$m_e \frac{dv_{\parallel}}{dt} = -e \frac{v_{\perp}}{c} B_z \quad \text{and}$$

$$m_e \frac{dv_{\perp}}{dt} = e \frac{v_{\parallel}}{c} B_z - \frac{ie}{kc} \frac{\partial B_z}{\partial t},$$

respectively, where the last term in the x_{\perp} component represents the force due to the inductive electric field. Therefore, the time derivative of the electric current flux is given by

$$\frac{\partial \langle j_{\perp} v_{\parallel} \rangle}{\partial t} = e^2 \frac{u^2}{cm_e} B_z,$$

where $j_{\perp} = -ev_{\perp}$ is the x_{\perp} component of the electric current carried by an single electron and $\langle X \rangle = \frac{1}{n_0} \int d^3v X(v) f(v)$ is the average over the velocity space. This current flux and the inductive electric field cause a change in the mean value of j_{\perp} as

$$\frac{\partial \langle j_{\perp} \rangle}{\partial t} = -\frac{\partial \langle j_{\perp} v_{\parallel} \rangle}{\partial x_{\parallel}} + e^2 i \frac{1}{m_e kc} \frac{\partial B_z}{\partial t}.$$

Ampère's law provides

$$n_0 \langle j_{\perp} \rangle = -\frac{ick}{4\pi} B_z,$$

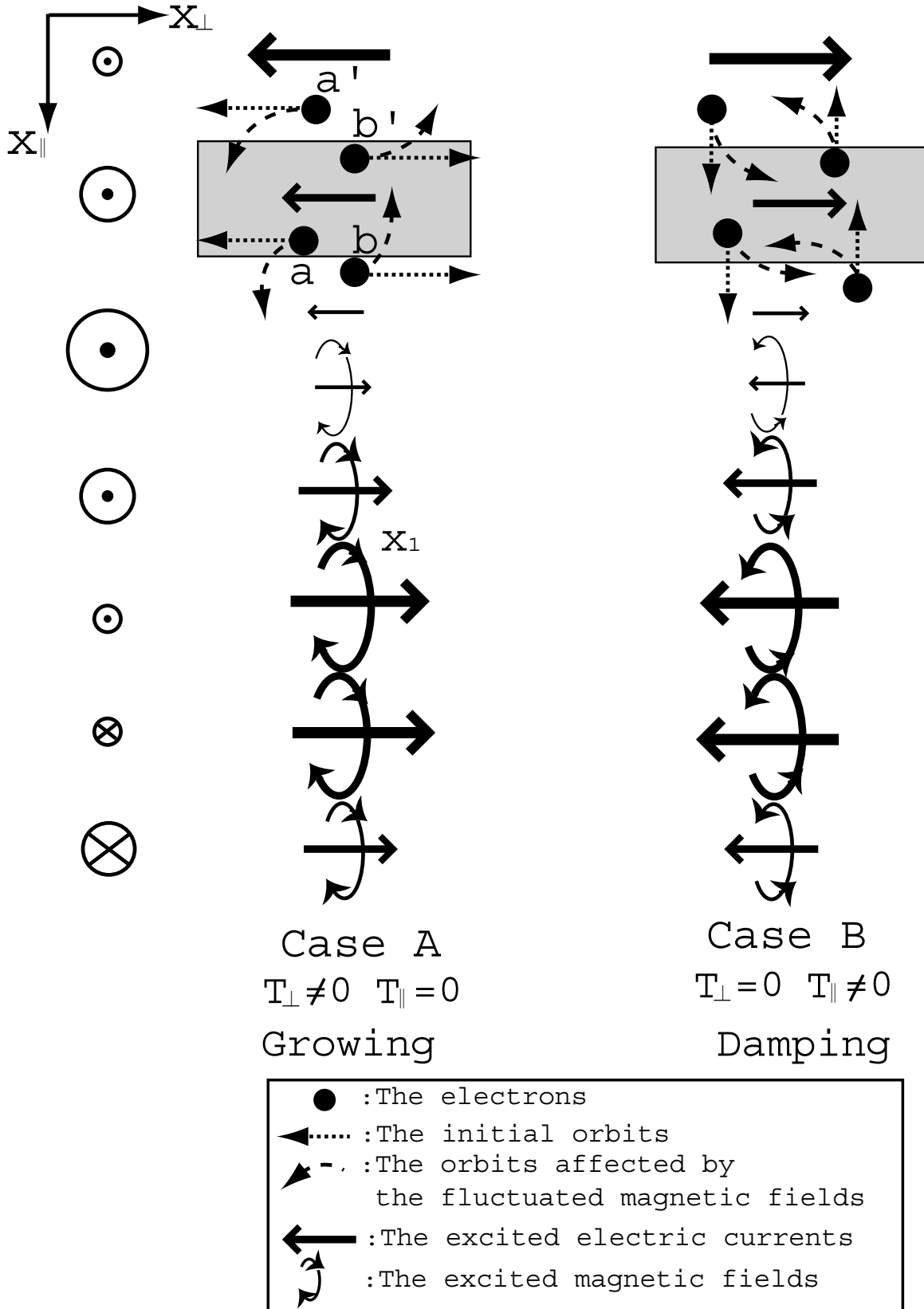


FIG. A4.— The physical mechanism of the Weibel instability.

where the displacement current is neglected since only the low frequency mode is considered. By combining these equations, we obtain

$$\left[1 + \frac{\omega_p^2}{c^2 k^2} \right] \frac{\partial^2 B_z}{\partial t^2} = \frac{\omega_p^2}{c^2} u^2 B_z.$$

The dispersion relation is obtained as

$$\gamma = \frac{(\omega_p/c)u}{\sqrt{1 + \frac{\omega_p^2}{c^2 k^2}}}.$$

It shows that the perturbation can grow. The second term in the [] of the left hand side comes from the induction term. Therefore, the electromagnetic induction actually plays a role in the inertia for the growth of the perturbation and reduces the growth rate, but never stops the growth of the perturbation. The obtained growth rate is exactly the same as the result deduced by the full linear analysis based on plasma kinetic theory where the induction effect is also taken into account (e.g., Melrose 1986).

References

- Arnaud, M., Aghanim, N., Gastaud, R., Neumann, D. M., Lumb, D., Briel, U.; Altieri, B., Ghizzardi, S., Mittaz, J., Sasseen, T. P. & Vestrand, W. T., 2001 *A&A*, 365, L67.
- Bacchi, M., Feretti, L., Giovannini, G. & Govoni, F., 2003, *A&A*, 400, 465.
- Biermann, L. 1950, *Zeit. Naturforschung*, 5a, 65.
- Blanton, E. L., Sarazin, C. L., McNamara, B. R. & Wise, M. W., 2001, *ApJ*, 558, L15.
- Briel, U. G., Henry, J. P. & Böhringer, H., 1992, *A&A*, 259, L31.
- Briel, U. G., Henry, J. P., Lumb, D. H., Arnaud, M., Neumann, D., Aghanim, N., Gastaud, R., Mittaz, J. P. D., Sasseen, T. P., & Vestrand, W. T, 2001, *A&A*, 365, L60.
- Carilli, C. L. & Taylor, G. B., 2002, *ARA&A*, 40, 319.
- Chapman, S. & Cowling, T. G. 1960, *The Mathematical Theory of Nonuniform Gases* (Cambridge: Cambridge Univ. Press)
- Clarke, T. E., Kronberg, P. P., & Böhringer, H., 2001, *ApJ*, 547, L111.
- De Young, D. S., 1992, *ApJ*, 386, 464.
- Elbaz, D., Arnaud, M. & Böhringer, H. 1995, *A&A*, 293, 337.
- Fabian, A. C., Sanders, J. S., Ettori, S., Taylor, G. B., Allen, S. W., Crawford, C. S., Iwasawa, K., Johnstone, R. M. & Ogle, P. M., 2000, *MNRAS*, 318, L65.
- Fabian, A. C., Voigt, L. M. & Morris, R. G., 2002, *MNRAS*, 355, L71.
- Feretti, L. 1999, in *Diffuse Thermal and Relativistic Plasma in Galaxy Clusters*, ed. H. Böhringer, L. Feretti, & P. Schuecker, *MPE Report* 271, 3.
- Feretti, L., Fusco-Femiano, R., Giovannini, G. & Govoni, F., 2001, *A&A*, 373, 106.
- Fried, B. D. 1959, *Phys. Fluids*, 2, 337.
- Fusco-Femiano, R., Orlandini, M., De Grandi, S., Molendi, S., Feretti, L., Giovannini, G., Bacchi, M. & Govoni, F., 2003, *A&A*, 398, 441.
- Gallev, A. A. & Natanzon, A. M. 1991, *Physics of laser plasma*, Chap. 13, ed. Rubenchik, A. & Witkowski, S., (Tokyo: North-Holland)
- Giovannini, G., Fereti, L., Venturi, T., Kim, K. T. & Kronberg, P. P., 1993, *ApJ*, 406, 399.
- Govoni, F., Feretti, G., Giovannini, H., Böhringer, H., Reiprich, T. H. & Murgia, M., 2001, *A&A*, 376, 803.
- Hattori, M. & Umetsu, K. 2000, *ApJ*, 533, 84.
- Jaffe, W., 1980, *ApJ*, 241, 925.
- Kim, K.T., Kronberg, P. P. & Tribble, P. C., 1991, *ApJ*, 379, 80.
- Krall, A. & Trivelpiece, A. W. 1973, *Principles of plasma physics* (New York: McGraw-Hill)
- Kulsrud, R. M., Cen, R., Ostriker, J. P. & Ryu, D., 1997, *ApJ*, 480, 481.
- Lee, R & Lampe, M. 1973, *Phy. Rev. Lett.*, 31, 1390.
- Levinson, A. & Eichler, D. 1992, *ApJ*, 387, 212
- Liang, H., Hunstead, R. W., Birkinshaw, M. & Andreani, P., 2000, *ApJ*, 544, 686.
- Markevitch, M., Ponman, T. J., Nulsen, P. E. J., Bautz, M. W., Burke, D. J., David, L. P., Davis, D., Donnelly, R. H., Forman, W. R., Jones, C., Kaastra, J., Kellogg, E., Kim, D.-W., Kolodziejczak, J., Mazzotta, P., Pagliaro, A., Patel, S., Van Speybroeck, L., Vikhlinin, A., Vrtilik, J., Wise, M., & Zhao, P., 2000, *ApJ*, 541, 542.
- Markevitch, M. & Vikhlinin, A., 2001, *ApJ*, 563, 95.
- Markevitch, M., Vikhlinin, A., Burke, D., Butt, Y., David, L., Donnelly, H., Forman, W. R., Harris, D., Kim, D.-W., Virani, S., & Vrtilik, J., 2003, *ApJ*, 586, 19.
- Mason, B. S. & Myers, S. T., 2000, *ApJ*, 540, 614.
- McNamara, B. R., Wise, M. W., Nulsen, P. E. J., David, L. P., Carilli, C. L., Sarazin, C. L., O’Dea, C. P., Houck, J., Donahue, M., Baum, S., Voit, M., O’Connell, R. W. & Koekemoer, A., 2001, *ApJ*, 562, L149.
- Melrose D.B. 1986, *Instabilities in Space and Laboratory Plasmas* (Cambridge: Cambridge Univ. Press)
- Morse R. L. & Nielson C. W. 1971, *Phys. Fluids.*, 14, 830.
- Okabe, N. & Hattori, M., 2003, *ApJ* in press, astro-ph/0308503.
- Okabe, N. & Hattori, M., in preparation.
- Ramani, A. & Laval, G. 1978, *Phys. Fluids.*, 21, 980.
- Rephaeli, Y. Gruber, D., & Blanco, P. 1999, *ApJ*, 511, L21.
- Rephaeli, Y. & Gruber, D., 2002, *ApJ*, 579, 587.
- Ruzmaikin, A., Sokolov, D. & Shukurov, A., 1989, *MNRAS*, 241, 1.
- Sarazin, C. L. 1988, *X-ray Emissions from Clusters of Galaxies* (Cambridge: Cambridge Univ. Press)
- Sentoku, Y., Mima, K., Kojima, S., Ruhl, H., 2000, *Phys. Plasma*, 7, 689.
- Sentoku, Y., Mima, K., Sheng, Z. M., Kaw, P., Nishihara, K. & Nishihara, K. 2002, *Phys. Rev. E.*, 65, 046408.
- Vikhlinin, A., Markevitch, M. & Murray, S. S. 2001a, *ApJ*, 551, 160.
- Vikhlinin, A., Markevitch, M. & Murray, S. S. 2001b, *ApJ*, 549, L47.
- Vikhlinin, A. & Markevitch, M. 2002, *AstL*, 28, 495.
- Wallace, J. M. & Epperlein, E. M. 1991, *Phys. Fluids B*, 3, 1579.
- Weibel, E. S. 1959, *Phys. Rev. Lett.*, 2, 83.
- Zakamska, N. L. & Narayan, R., 2003, *ApJ*, 582, 162.